Molecular simulation of displacement of shale gas by carbon dioxide at different geological depths

Haibo Zhang [a], Dapeng Cao [a,b,*]

[a] State Key Lab of Organic Inorganic Composites, Beijing University of Chemical Technology, Beijing 100029, PR China
[b] International Research Center for Soft Matter, Beijing University of Chemical Technology, Beijing 100029, PR China

HIGHLIGHTS

- We investigate the displacement of shale gas by carbon dioxide at different conditions.
- The increase of pore size is beneficial for the displacement of shale gas.
- The optimum operating conditions of carbon dioxide displacing shale gas are recommended.

GRAPHICAL ABSTRACT
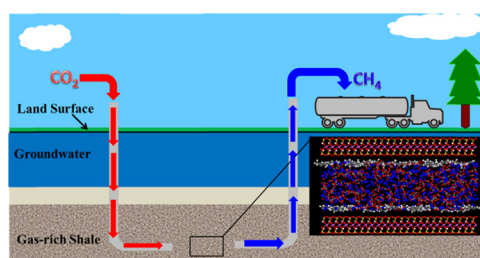
ABSTRACT

The rising worldwide energy demand has greatly stimulated the exploitation of shale gas. Meantime, global warming mainly caused by CO_2 emission is a significant concern. As a new scenario, injecting CO_2 to displace shale gas is proposed to improve the exploitation efficiency of shale gas and reduce the amount of CO_2 emission. In this work, we use a grand canonical Monte Carlo simulation to investigate the displacement of shale gas by CO_2 and the sequestration of CO_2 simultaneously in a modeled shale matrix at different geological depths from 1 to 4 km, where the shale is modeled by inorganic clay mineral and organic matter. We find that both the displacement amount of CH_4 and the sequestration amount of CO_2 increase with the pore size of the shale at a fixed CO_2 injection pressure, which suggests that the hydro-fracturing technology would be very beneficial for displacement exploitation of shale gas. Moreover, we also find that the optimum operating condition for CO_2 displacing shale gas is at the depth of 1 km, which provides a guidance and reference for displacement exploitation of shale gas by CO_2.

© 2016 Elsevier Ltd. All rights reserved.

1. Introduction

Recently, the exploration and development of shale gas have received extensive attention worldwide because of its numerous advantages such as low pollution, wide distribution, and abundant resource (Howarth et al., 2011). Shale gas, as an unconventional gas source, refers to a kind of natural gas that exists in shale reservoirs (Shaikh and Ji, 2016; Youinou, 2016), and is now increasingly deemed as a low carbon and an environmentally friendly energy option. The United States of America (USA) is the earliest country to apply the horizontal drilling and hydro-fracturing into the exploration and development of shale gas (Arora and Cai, 2014; Connor et al., 2015). The output of shale gas has reached 13.78 billion cubic meters per year in USA, with an average annual growth rate of 47.7% (Zhai et al., 2014), while, the natural gas from shale formations is about 23% in 2010. And, it is anticipated to contribute 49% of gas production by 2035 (Ashmoore et al., 2016). In order to reduce pollution and meet a surge in energy demand, China aims to produce 30 billion cubic meters of shale gas per year by 2020, from the current level of 1.3 billion

---

* Correspondence to: State Key of Organic Inorganic Composites, Beijing University of Chemical Technology, Beijing 100029, PR China. Tel: +86 10 64443254.
E-mail address: caodp@mail.buct.edu.cn (D. Cao).

cubic meters (Wang et al., 2016). Therefore, considerable efforts are undertaken by Chinese enterprises through the development of research programs in industry to make this resource successfully and economically available (Gasparik et al., 2012).

Currently, the ultralow porosity of shale and ultralow permeability of gas reservoirs are still a great challenge in the exploration of shale gas (Clarkson et al., 2016). Hydro-fracturing is a commonly used method to enhance matrix permeability of unconventional reservoirs and enable the economic production of shale gas from the shale reservoirs (Chen and Carter, 2016; Clark et al., 2012; Clarkson et al., 2016). However, the hydro-fracturing would cause severe environment impacts, e.g. huge water consumption, potential contamination of water and so on (Clark et al., 2012; Connor et al., 2015; Krogulec and Sawicka, 2015; Krupnick and Gordon, 2015). Alternatively, the new scenario, the injection of CO_2 gas to displace the adsorbed CH_4, has been proposed by some researchers (Kowalczyk et al., 2012; Shi and Durucan, 2003; Wang et al., 2015b; Wu et al., 2015; Yu et al., 2008). It arouses extensive interests from scientists, because it can improve the shale gas recovery and sequestrate CO_2 simultaneously.

Most studies on the displacement of CH_4 adsorbed in shale matrix by CO_2 have been carried out by the experiment and computation at present. Wu (Wu et al., 2015) studied the displacement of CH_4 in carbon nanochannels by molecular dynamics (MD) simulations. And they drew a conclusion that CO_2 can displace the adsorbed CH_4 directly. Yuan (Yuan et al., 2015) also explored the displacement of CH_4 by injecting CO_2 on graphene, and found that CO_2 can be adsorbed on graphene more easily than CH_4, which may be a good candidate for displacement of CH_4. Pathak (Pathak et al., 2015) performed MD simulations on the kerogen-methane-carbon dioxide system to understand the absorption-adsorption- desorption phenomena of the super critical CO_2 fluid, and found that CO_2 can sweep the absorbed CH_4 from the kerogen matrix in the shales. Kowalczyk (Kowalczyk et al., 2012) investigated displacement of CH_4 by Monte Carlo simulations, and proposed two-stage mechanism for the displacement of CH_4 from carbon nanospaces by coadsorbed CO_2. Wang (Wang et al., 2015a) conducted experiments to study the coal-bed CH_4 displacement by CO_2 injection, and found that the adsorption capacity of CO_2 is stronger than that of CH_4 under the same condition in the process of displacement.

A large proportion of pores within the gas shale matrix are nanosized, and most of these pores are associated with the constituents of the shale matrix and the contents of each components (Cui et al., 2009). In addition, the shale matrix often contains some free gases in relatively large pores and adsorbed gas on the organic matter and inorganic minerals (Zhang et al., 2012). To deal with the complex situation, it is necessary to simplify the complicated structure of shale matrix to gain some basic insights into its adsorption behavior. There are two ways to address this topic in the literatures. One is to assume the clay-rich shale as the crystal structure of montmorillonite with the basal spacing and number of ions changing (Zhai et al., 2014). The disadvantage of this method does not include the organic matter. In fact, the organic matter is an indispensable factor on the CH_4 adsorption in shale matrix. The other method is to model the complex natural matrixes as a collection of independent, on-interconnected slit pores with perfect graphitic walls without consideration of inorganic minerals (Hu et al., 2011). As a result, it is important to construct an all-atom shale model including inorganic minerals and organic matter to investigate the adsorption and displacement of CH_4 in gas shale matrix.

In this work, we proposed a modified and generalized shale matrix model including inorganic minerals and organic matter. Then, the mechanism of the displacement of CH_4 by CO_2 in shale matrix model was investigated through molecular simulations. Finally, some discussion was also addressed.

2. Computational details

2.1. Models and potentials

Since CH_4 is the major component of shale gas, we use it to represent the shale gas. The components of gas shale matrix include organic matter, inorganic clay minerals, quartz, carbonate, calcite, pyrite, and the others (Tan et al., 2014). The main ingredients in the gas shale matrix from different places are nearly the same, but their contents of the components are different. Here, we mainly consider the case of CH_4 in shale matrix, which contains organic matter and inorganic clay minerals. To construct the shale matrix model containing inorganic clay mineral and organic matter, we used two perfect montmorillonite sheets to represent the inorganic clay mineral. Montmorillonite is a typical 2:1 inorganic clay mineral, and the unit cell consists of an $Al-O$ octahedral sheet and two $Si-O$ tetrahedral sheets, while the $Al-O$ sheet is sandwiched between $Si-O$ sheets. Generally, it is believed that the polycyclic aromatic hydrocarbon is a major organic component of shale matrix, especially for shale gas reservoirs. Therefore, we used methylnaphthalene to represent the organic matter in the shale matrix here.

We constructed a simulation box ($31.1 \times 35.9 \times c$ Å) that contains two inorganic layers and two organic layers (see Fig. 1). As mentioned above, the perfect montmorillonite sheets were used to represent the inorganic layers. The structure of the montmorillonite sheets was obtained from the Cambridge Crystallographic Data Centre (CCDC) database. First, two perfect montmorillonite sheets were stacked each other in such a way as shown in Fig. 1. Then, a set of methylnaphthalene molecules were absorbed into the interlayer space, where the pore size of our model was adjustable through the basal spacing. The methylnaphthalene molecules absorbed into the interlayer space were fixed, as the
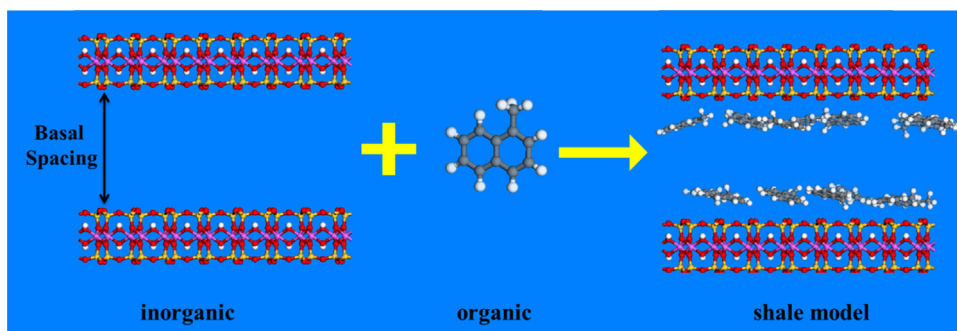

Fig. 1. The scheme of modeled shale matrix. Color scheme: red, oxygen; yellow, silicon; pink, aluminum; white, hydrogen; and black, carbon.

organic matter in shale matrix. During our simulations, the shale matrix model containing organic and inorganic matter was treated as a rigid material with atoms frozen.

In this work, CH_4 was represented by a spherical united-atom model (Cao et al., 2003; Lan et al., 2010), CO_2 was modeled as a three-site rigid linear molecule with three charged Lennard-Jones (LJ) interaction sites (Liu and Wilcox, 2013). The potential parameters were taken from the transferable potentials for phase equilibrium (TraPPE) model (Jorgensen et al., 1996). The realistic CLAYFF force field (Cygan et al., 2004) for inorganic clay minerals in the shale matrix model was used in this work, and the Dreiding force field (Mayo et al., 1990) was adopted for the organic matter in the shale matrix model. The site-site LJ potentials were adopted to calculate the CH_4–CH_4 and CH_4-shale intermolecular interactions. In addition, when calculating the CO_2–CO_2 and CO_2-shale intermolecular interactions, the Coulombic potentials were added. In the MUSIC software, to avoid the conversion of chemical potential into pressure, the normal move acceptance probability was transformed to relate with the component fugacity of gas bulk phase, which was calculated by the Peng−Robinson equation of state (EOS) (Peng et al., 2011). All the Lennard−Jones (LJ) cross-interaction parameters were determined by the Lorentz−Berthelot mixing rules [$\sigma_{ij}=(\sigma_{ii}+\sigma_{jj})/2$ and $\varepsilon_{ij}=(\varepsilon_{ii} \cdot \varepsilon_{jj})^{1/2}$], where corresponding parameters are shown in Table 1.

2.2. Grand canonical Monte Carlo simulations

The grand canonical Monte Carlo (GCMC) simulations were used to investigate the displacement of CH_4 in shale matrix at different geological depths. First, the CH_4 molecules were pre-adsorbed into the nanochannels of the shale matrix. The partial pressure of CH_4 in the binary CH_4-CO_2 bulk mixture, which is corresponding to the geological pressure condition of shale gas, determines the preadsorption amount of CH_4 in the shale matrix. Then, we injected a small amount of CO_2 molecules into the bulk CH_4 gas and equilibrated the resulting mixture in the shale reservoirs. After equilibration, the adsorption amounts of CO_2 and CH_4 in shale matrix were calculated by analyzing the compositions of the adsorbed mixture. Finally, we gradually increased the CO_2 partial pressure (i.e. CO_2 injection pressure) in the binary CH_4-CO_2 bulk mixture up to 90 MPa, which makes it possible to study the microscopic mechanism of the displacement of CH_4 from the shale matrix. In each case, 2×10^7 configurations were generated. The first half is for the system to reach the equilibrium, whereas the second half is for sampling.

In the displacement process of CH_4 by CO_2, the displacement amount of CH_4 is defined as

$$N_{displacement} = N_{initial} - N_{P_{CO_2}} \tag{1}$$

The percentage of displacement is defined as

$$\eta_{displacement} = \frac{N_{initial} - N_{P_{CO_2}}}{N_{initial}} \tag{2}$$

Where $N_{initial}$ and $N_{P_{CO_2}}$ denote absolute amount of CH_4 adsorbed in the nanochannel of shale matrix when the partial pressure of CO_2 in bulk mixture is equal to zero (i.e. pure CH_4) and P_{CO_2}, respectively.

The pore volume of the adsorbent accessible to the gas molecule is calculated by the method of Myers from the ideal gas law (Talu and Myers, 2001)

$$V_{pore} = \frac{RN_mT}{pm_m} \tag{3}$$

where R is the gas constant, T is the temperature, p is the pressure, and N_m is the number of adsorbed probe molecules per molar mass of the adsorbents, which is obtained from the GCMC simulations of non-adsorbed helium ($\varepsilon_{He}/K_b=10.22$ K; $\sigma_{He}=2.85$ Å) gas in shales at low pressure and ambient temperature.

The temperatures and pressures corresponding to the specific geological depths were introduced in the simulations to reproduce the T/P conditions encountered in a typical sedimentary basin, mainly based on the fact that the compacting stress gradient is 15 MPa/km and the geothermal gradient is 30 K/km (Cygan et al., 2004; Titiloye and Skipper, 2005). The T/P conditions were listed in Table 2. All the GCMC simulations were performed by using the computational packages MUSIC (Gupta et al., 2003).

3. Results and discussion

3.1. Modeling

The total organic content and basal spacing of the shale matrix model were determined by fitting the experimental and simulation data. To validate the simulated data and the model, we made a series of comparisons with available experimental data from the literature. An experimental adsorption isotherm of CH_4 in the shale with the total organic content of 5.08%, was measured at 363 K by Zeng et al. (Zeng et al., 2014). In agreement of the total organic content of shale matrix with the experimental sample, fourteen methylnaphthalene molecules were absorbed into the slit pore formed by two perfect montmorillonite sheets. Then, a series of adsorption isotherms of CH_4 in the shale model with different basal spacing were simulated at 363 K. By comparing the GCMC simulated isotherms and experimental one (see Fig. 2), we could determine the basal spacing about 7 Å for the shale model. The simulated pore volume of our shale model is 0.0173 cm³/g, which is consistent with the experimental result of 0.0162−0.0448 cm³/g (Clarkson et al., 2013). So, we believe that the shale model proposed here is rational, and further use the model to investigate the displacement of CH_4 by CO_2 in the shale matrix.

3.2. The Displacement of Shale Gas by Carbon Dioxide at Different Basal Spacings

First, we used GCMC simulations to investigate the displacement

Table 1
Force field parameters for adsorbates and adsorbents.

molecules		atoms	charge[e]	σ[Å]	$\varepsilon/k_B[K]$
Methane		CH_4	0	3.73	148
Carbon Dioxide		C	0.70	2.80	27
		O	−0.35	3.05	79
Shale	Inorganic	H	0.424		
		O(octahedral)	−1.424	3.55	78.26
		O(tetrahedral)	−0.8	3.55	78.26
		O(apical)	−1.0	3.55	78.26
		Al	3.0	4.79	0.0007
		Si	1.2	3.71	0.0009
	Organic	C	–	3.47	47.9
		H	–	2.85	7.7

Table 2
Temperature and Pressure Conditions in Different Geological Depths.

case	depth	T	P
Case 1	1 km	310 K	15 MPa
Case 2	2 km	340 K	30 MPa
Case 3	3 km	370 K	45 MPa
Case 4	4 km	400 K	60 MPa

of CH_4 by CO_2 in the shale at geological depth of 1 km, in which the partial pressure of CH_4 and the temperature are 15 MPa and 310 K, respectively, corresponding to the condition of the shale gas at the geological depth of 1 km (i.e. Case 1 in Table 2). Then, we injected CO_2 into the shale, and the CO_2 injection pressure is increased from 0 to 90 MPa. After equalization, the composition of the adsorbed mixture is further recorded and analyzed.

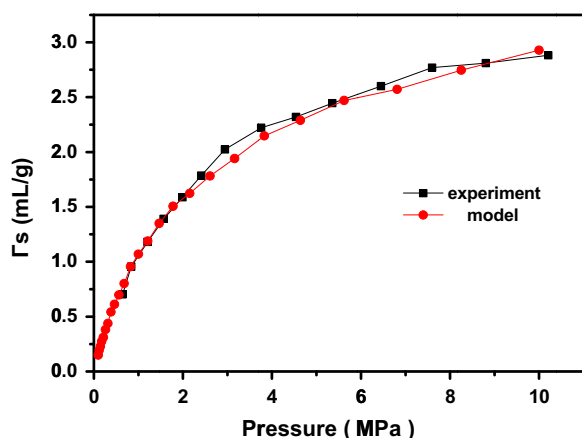To explore the effect of pore size on the displacement of CH_4 by

Fig. 2. Adsorption isotherms of CH_4 in the shales from experiment and simulation at T = 363 K.

CO_2 in shale, we explored a series of modeled shales with different basal spacings. Fig. 3a and b show the loading amount of CH_4 and the sequestration amount of CO_2 in the nanochannels of the shale at different CO_2 injection pressures. With the increase of CO_2 injection pressure, the loading amount of CH_4 in the shale decreases monotonically except for the case of 100 Å, and the sequestration amount of CO_2 goes up steadily, which means the CH_4 adsorbed in the shale nanochannel is displaced by CO_2 and it is sequestrated simultaneously in the shale nanochannels. The reason for this phenomenon is that the shale nanochannel has stronger affinity to CO_2 than to CH_4, and shows selective adsorption for CO_2. As a result, the CH_4 molecules adsorbed in the nanochannel surfaces of shales are displaced by CO_2 molecules, and the CH_4 molecules are pushed back to the bulk phase finally.

A peak is observed in the case of the basal spacing 100 Å in Fig. 3a. At low CO_2 injection pressure, the adsorbed CO_2 molecules induced the enhancement of CH_4 adsorption compared with the pure CH_4 adsorption; while at high CO_2 injection pressure, the displacement of CH_4 by CO_2 is pronounced. This phenomenon was also observed in the work of Kowalczyk et al.(Kowalczyk et al., 2012). At low CO_2 injection pressure, some additional CH_4 molecules are pumped from the bulk mixture gas into the shale. The adsorbed CO_2 molecules can be acted as a part of the external field that overall enhances the solid-fluid interactions with bulk CH_4 molecules (Kowalczyk et al., 2012), which leads to the slight increase of adsorption amount of CH_4.

It is noted that the basal spacing of the shale model, i.e. the pore size, is crucial to the displacement amount of CH_4 and the

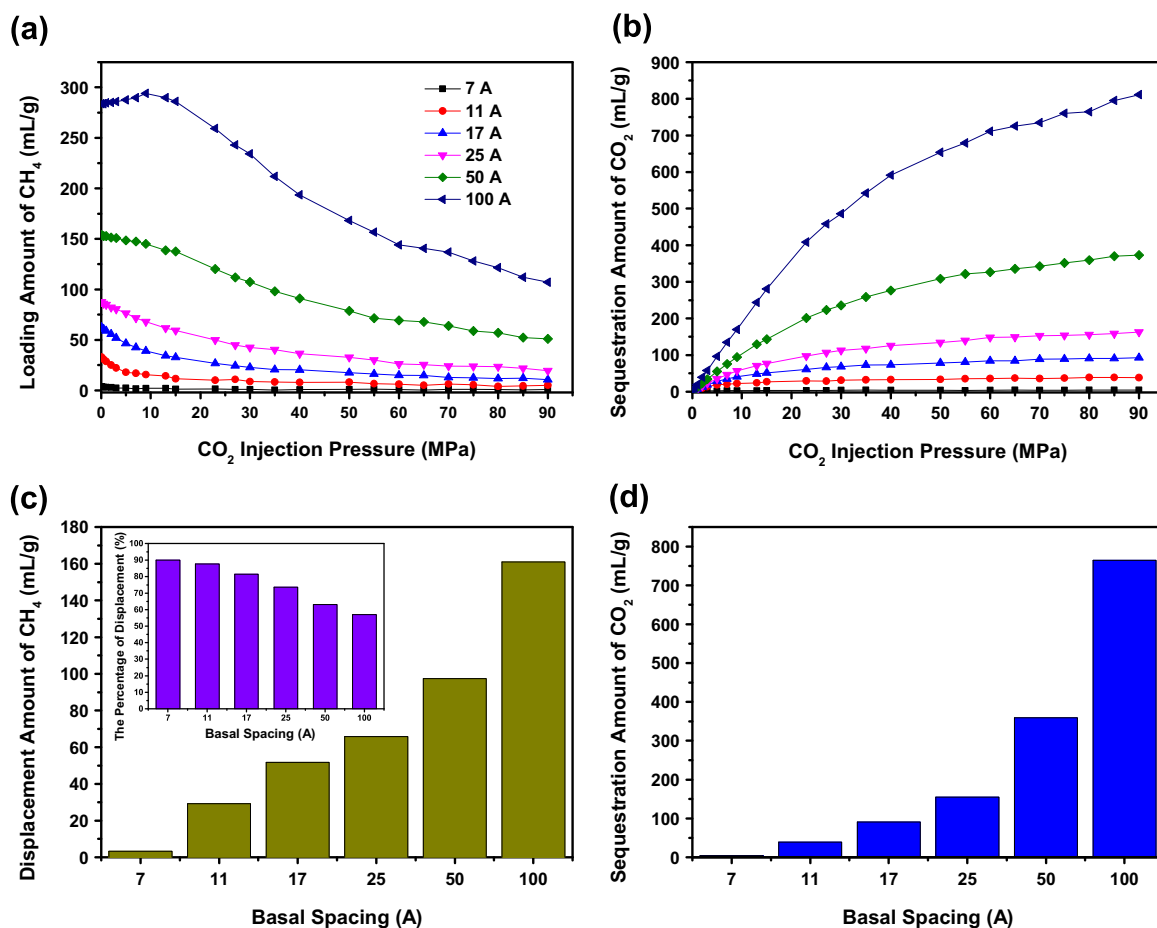**Fig. 3.** (a) The loading amount of CH_4 and(b) the sequestration amount of CO_2 in the modeled shales at different CO_2 injection pressures and T = 310 K, where the partial pressure of CH_4 is fixed at 15 MPa, corresponding to the pressure condition of shale gas at the geological depth of 1 km, and the CO_2 injection pressure is increased gradually from 0 to 90 MPa.(c) the displacement amount of CH_4, and the inset of (c) is the percentage of displacement at the CO_2 injection pressure of 80 MPa and T = 310 K. (d) the sequestration amount of CO_2.
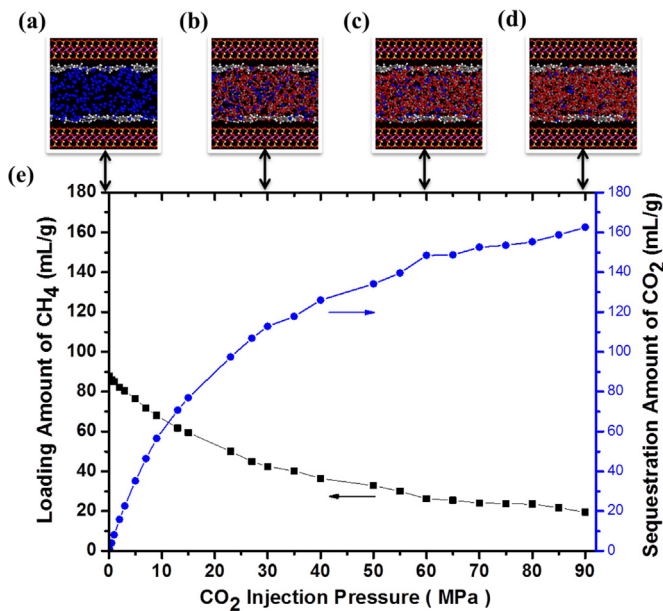
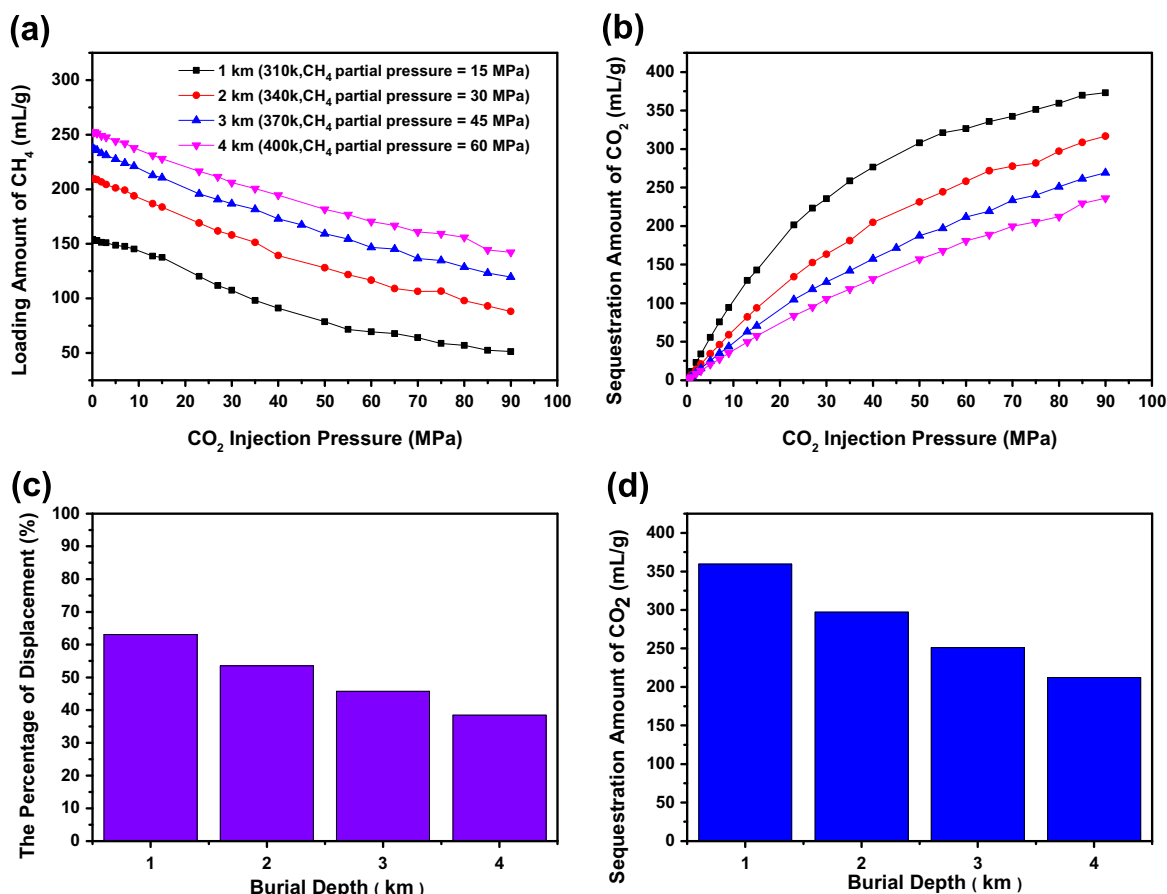**Fig. 4.** The snapshots of the binary CO_2-CH_4 mixtures adsorbed in the pore of shales at T=310 K and different CO_2 injection pressures,(a) 0, (b) 30 MPa, (c) 60 MPa, (d) 90 MPa. In all presented snapshots, the CH_4 partial pressure of 15 MPa is kept fixed in the bulk mixture. The basal spacing of shale model is set to be 25 Å. Color scheme: red, oxygen; black, carbon; blue, methane; yellow, silicon; pink, aluminum and white, hydrogen. (e) The loading of CH_4 and the sequestration of CO_2 at different CO_2 injection pressures.

sequestration of CO_2 in shales. For further explanation, Fig. 3c and d show the displacement amount of CH_4 and the sequestration amount of CO_2 at the CO_2 injection pressure of 80 MPa. The shale gas reservoirs often contain the free gas in relatively large pores and the adsorbed gas associated with organic matters and inorganic minerals. Both free and adsorbed gases are important for application of exploitation of shale gas. Hence, the absolute amount is more significant than the excess amount for estimating the storage of shale gas reservoirs. With the increase in the basal spacing of the shale model, the displacement amount of CH_4 and the sequestration amount of CO_2 are increased sharply (see Fig. 3c and d). In fact, the increase of the basal spacing in the shale model will result in the enhancement of the pore volume. As a result, the absolute amount of CH_4 and CO_2 adsorbed in relatively large pores will be increased significantly. When CH_4 is displaced by CO_2 at the CO_2 injection pressure of 80 MPa, the displacement amount of CH_4 and the sequestration amount of CO_2 in relatively large pores exceed that in relatively small pores obviously (see Fig. 3c and d).

It is found from the inset of Fig. 3c that the percentage of displacement is inversely proportional to the basal spacing of shale model (i.e. pore size). The reason could be that the enlargement of basal spacing reduces the selectivity of the shale for CO_2 over CH_4. That is to say, the affinity of the inner surface to CO_2 in relatively small pores is stronger than that in relatively large pores. So, as the basal spacing of shale model increases gradually, the percentage of displacement goes down slightly. However, the displacement amount of CH_4 is more important than the percentage of displacement for the exploitation of shale gas.
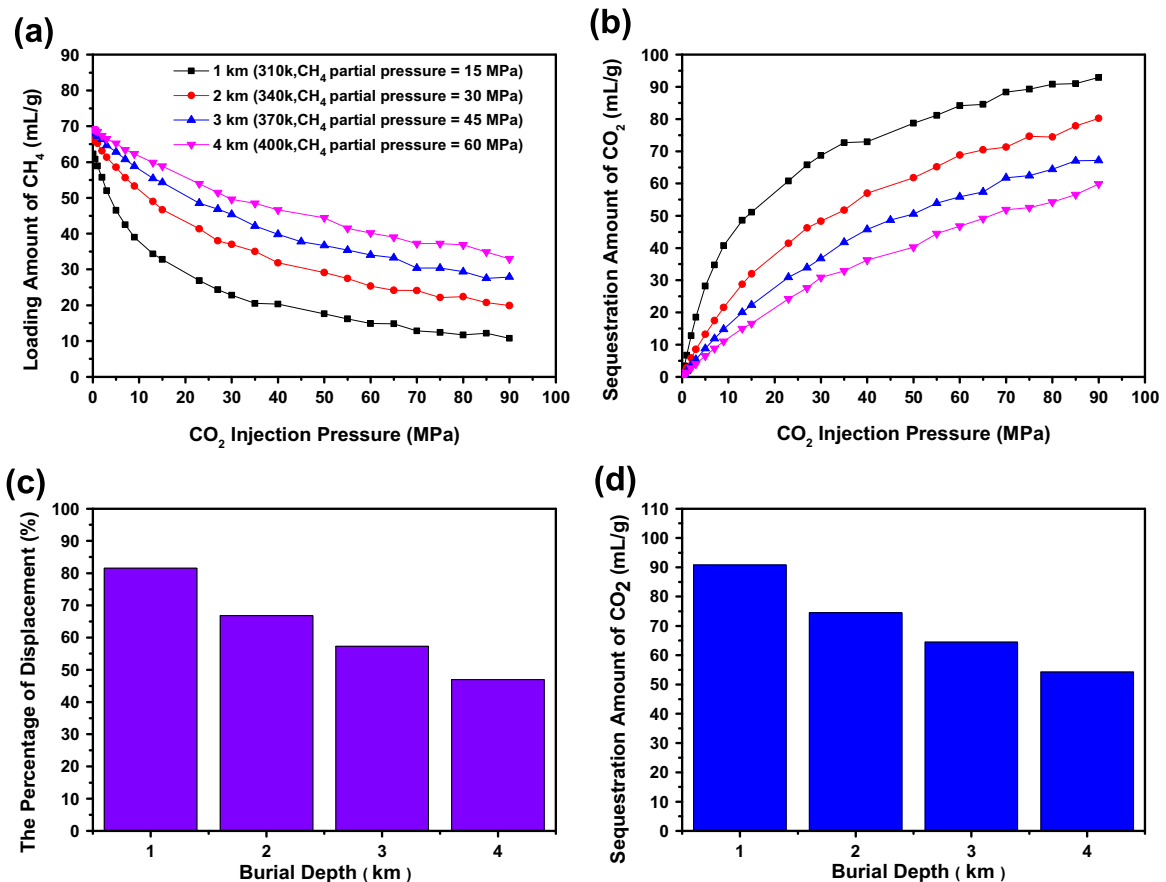
Fig. 5. (a) The loading amount of CH_4 and (b) the sequestration amount of CO_2 in shales at different CO_2 injection pressures and different geological depths. (c) The percentage of displacement and (d) the sequestration amount of CO_2 in shale at the CO_2 injection pressure of 80 MPa. The basal spacing of shale model is 17 Å (micropores).

Fig. 6. (a) The loading amount of CH_4 and (b) the sequestration amount of CO_2 in shales at different CO_2 injection pressures and different geological depths. (c) The percentage of displacement and (d) the sequestration amount of CO_2 in shale at the CO_2 injection pressure of 80 MPa. The basal spacing of shale model is 50 Å (mesopores).

To get an insight into the microscopic behavior of CH_4 displaced by CO_2 in shale, Fig. 4a-d show microscopic snapshots of the binary CO_2-CH_4 mixtures adsorbed in the nanochannels of shales at the CO_2 injection pressure of 0, 30, 60, 90 MPa, respectively, in which the CH_4 partial pressure of 15 MPa and T=310 K are fixed, and the basal spacing of the shale model is 25 Å. For comparison, Fig. 4e shows the loading amount of CH_4 and the sequestration amount of CO_2 in the shales at different CO_2 injection pressures. At the CO_2 injection pressure of 0 MPa (i.e. the initial state), the nanochannels are fully filled with CH_4 molecules (Fig. 4a). As CO_2 is injected into the shale, a certain amount of CO_2 is also adsorbed and a part of CH_4 molecules are driven out from the nanochannels (Fig. 4b-d). The dynamic process is also presented in Supporting Information Video.

Supplementary material related to this article can be found online at http://dx.doi.org/10.1016/j.ces.2016.09.002.

3.3. The displacement of shale gas by carbon dioxide at different geological depths

In this section, the influence of the geological depths on the displacement of CH_4 by CO_2 was studied. The T/P conditions corresponding to the specific geological depth were listed in Table 2. Based on the fact that a large proportion of the pores within the gas shale matrix is nanosized, we take into account not only the micropores (17 Å) but also the mesopores (50 Å). The displacement of CH_4 by CO_2 in micropores (17 Å) was investigated first (see Fig. 5). Fig. 5a shows the relationship between the loading amount of CH_4 in the shale and the CO_2 injection pressure at different geological depths. It is found that the geological depth plays a key

role in the displacement of CH_4 by CO_2. At the CO_2 injection pressure of 0 MPa (i.e. the initial state), the loading amounts of CH_4 in the shales from 1 to 4 km are nearly close with a slight difference. When CO_2 gas is injected into the shale, the loading of CH_4 in the shale goes down gradually. If the CO_2 injection pressure is kept the same, the loading reduction of CH_4 in the shales at the geological depth of 1 km is maximal in the four cases. If we only considered the displacement amount of CH_4, the geological depth of 1 km is the best choice in all the cases studied here. In addition, the sequestration amount of CO_2 is as important as the displacement of CH_4. Fig. 5b shows the sequestration amount of CO_2 versus the CO_2 injection pressure at the geological depths from 1 to 4 km. As expected, the sequestration amount of CO_2 increases with the CO_2 injection pressure (see Fig. 5b), while it decreases with the increase of geological depth at a fixed CO_2 injection pressure (see Fig. 5d). That is to say, the sequestration of CO_2 is maximum at geological depth of 1 km in all the four cases studied (Fig. 5d). Actually, the effect of CO_2 injection pressure on the displacement of shale gas is significant. The higher the CO_2 partial pressure, the larger is the displacement amount of CH_4 and the sequestration amount of CO_2. Interestingly, at the geological depth of 1 km, the percentage of displacement at the CO_2 injection pressure of 80 MPa is also the maximum among the four cases studied (see Fig. 5c). Consequently, it is concluded that by considering the displacement of CH_4, the sequestration of CO_2 and the percentage of displacement in the shales, we found that it is at the geological depth of 1 km that the displacement efficiency of CH_4 in shales by CO_2 is the highest.

We also studied mesopores by adjusting the basal spacing of shale model from 17 to 50 Å (see Fig. 6), and a similar

phenomenon with the microporous shales appears. Finally, we propose that the optimum operating condition that the CO_2 gas displaces the CH_4 gas in the shales, is under the geological depth of 1 km no matter what the shales are microporous or mesoporous, which would provide significant information and reference for displacement exploitation of shale gas and sequestration of CO_2.

4. Conclusion

We have used GCMC simulation to investigate the displacement of shale gas by CO_2 and the sequestration of CO_2 simultaneously in a modeled shale matrix at different geological depths up to 4 km. the shale model was constructed by organic-inorganic composites, and the rationality of the shale model was evaluated by fitting the experiment data. The results indicate that the CO_2 molecules can displace the shale gas adsorbed in the shales efficiently and the CO_2 is sequestrated into the shales simultaneously. It is found that the pore size, i.e. basal spacing, plays an important role in the displacement of CH_4 by CO_2. Interestingly, both the displacement amount of CH_4 and the sequestration amount of CO_2 increase with the pore size of the shales. However, with the increase of the geological depth, all the displacement amount of CH_4, the percentage of displacement and the sequestration amount of CO_2 decrease obviously. Accordingly, we suggest that the geological depth of 1 km is the optimum operating condition for the displacement of CH_4 by CO_2 in the shales discussed here. It is expected that this work would provide microscopic fundamentals and significant reference for displacement exploitation of shale gas and sequestration of CO_2.

Acknowledgment

References

Arora, V., Cai, Y., 2014. U.S. natural gas exports and their global impacts. Appl. Energy 120, 95–103.

Ashmoore, O., Evensen, D., Clarke, C., Krakower, J., Simon, J., 2016. Regional newspaper coverage of shale gas development across Ohio, New York, and Pennsylvania: Similarities, differences, and lessons. Energy Res. Soc. Sci. 11, 119-132.

Cao, D., Zhang, X., Chen, J., Wang, W., Yun, J., 2003. Optimization of Single-Walled Carbon Nanotube Arrays for Methane Storage at Room Temperature. J. Phys. Chem. B 107, 13286–13292.

Chen, H., Carter, K.E., 2016. Water usage for natural gas production through hydraulic fracturing in the United States from 2008 to 2014. J. Environ. Manag. 170, 152–159.

Clark, C., Burnham, A., Harto, C., Horner, R., 2012. Hydraulic fracturing and shale gas production: Technology, impacts, and policy. Argonne National. Lab. Sep, 10.

Clarkson, C., Haghshenas, B., Ghanizadeh, A., Qanbari, F., Williams-Kovacs, J., Riazi, N., Debuhr, C., Deglint, H., 2016. Nanopores to Megafractures: Current Challenges and Methods for Shale Gas Reservoir and Hydraulic Fracture Characterization. J. Natural Gas Sci. Eng. 31, 612-657.

Clarkson, C.R., Solano, N., Bustin, R.M., Bustin, A.M.M., Chalmers, G.R.L., He, L., Melnichenko, Y.B., Radliński, A.P., Blach, T.P., 2013. Pore structure characterization of North American shale gas reservoirs using USANS/SANS, gas adsorption, and mercury intrusion. Fuel 103, 606–616.

Connor, J., Molofsky, L., Richardson, S., Bianchi-Mosquera, G., 2015. Environmental Issues and Answers Related to Shale Gas Development. SPE Lat. Am. Caribb. Health, Saf., Environ. Sustain. Conf., 7–8.

Cui, X., Bustin, A.M.M., Bustin, R.M., 2009. Measurements of gas permeability and diffusivity of tight reservoir rocks: different approaches and their applications. Geofluids 9, 208–223.

Cygan, R.T., Liang, J.-J., Kalinichev, A.G., 2004. Molecular models of hydroxide, oxyhydroxide, and clay phases and the development of a general force field. J. Phys. Chem. B 108, 1255–1266.

Gasparik, M., Ghanizadeh, A., Bertier, P., Gensterblum, Y., Bouw, S., Krooss, B.M., 2012. High-Pressure Methane Sorption Isotherms of Black Shales from The Netherlands. Energy Fuels 26, 4995–5004.

Gupta, A., Chempath, S., Sanborn, M.J., Clark, L.A., Snurr, R.Q., 2003. Object-oriented programming paradigms for molecular modeling. Mol. Simul. 29, 29–46.

Howarth, R.W., Santoro, R., Ingraffea, A., 2011. Methane and the greenhouse-gas footprint of natural gas from shale formations. Clim. Change 106, 679–690.

Hu, X., Radosz, M., Cychosz, K.A., Thommes, M., 2011. CO_2-filling capacity and selectivity of carbon nanopores: synthesis, texture, and pore-size distribution from quenched-solid density functional theory (QSDFT). Environ. Sci. Technol. 45, 7068–7074.

Jorgensen, W.L., Maxwell, D.S., Tirado-Rives, J., 1996. Development and testing of the OPLS all-atom force field on conformational energetics and properties of organic liquids. J. Am. Chem. Soc. 118, 11225–11236.

Kowalczyk, P., Gauden, P.A., Terzyk, A.P., Furmaniak, S., Harris, P.J.F., 2012. Displacement of Methane by Coadsorbed Carbon Dioxide Is Facilitated In Narrow Carbon Nanopores. J. Phys. Chem. C. 116, 13640–13649.

Krogulec, E., Sawicka, K., 2015. Groundwater protection in shale gas exploration areas-a Polish perspective. Episodes 38, 9–20.

Krupnick, A.J., Gordon, H.G., 2015. What Experts Say About the Environmental Risks of Shale Gas. Dev. Agric. Resour. Econom. Rev. 44, 106–119.

Lan, J., Cao, D., Wang, W., 2010. High uptakes of methane in Li-doped 3D covalent organic frameworks. Langmuir 26, 220–226.

Liu, Y., Wilcox, J., 2013. Molecular simulation studies of CO_2 adsorption by carbon model compounds for carbon capture and sequestration applications. Environ. Sci. Technol. 47, 95–101.

Mayo, S.L., Olafson, B.D., Goddard, W.A., 1990. DREIDING: a generic force field for molecular simulations. J. Phys. Chem. 94, 8897–8909.

Pathak, M., Pawar, G., Huang, H., Deo, M.D., 2015. Carbon Dioxide Sequestration and Hydrocarbons Recovery in the Gas Rich Shales: An Insight from the Molecular Dynamics Simulations, Carbon Management. Technol. Conf. Nov., 17–19.

Peng, X., Cheng, X., Cao, D., 2011. Computer simulations for the adsorption and separation of CO_2/CH4/H2/N2 gases by UMCM-1 and UMCM-2 metal organic frameworks. J. Mater. Chem. 21, 11259.

Shaikh, F., Ji, Q., 2016. Forecasting natural gas demand in China: Logistic modelling analysis. Int. J. Electr. Power Energy Syst. 77, 25–32.

Shi, J.Q., Durucan, S., 2003. A bidisperse pore diffusion model for methane displacement desorption in coal by CO_2 injection. Fuel 82, 1219–1229.

Talu, O., Myers, A.L., 2001. Molecular simulation of adsorption: Gibbs dividing surface and comparison with experiment. AIChE J. 47, 1160–1168.

Tan, J., Horsfield, B., Fink, R., Krooss, B., Schulz, H.-M., Rybacki, E., Zhang, J., Boreham, C.J., van Graas, G., Tocher, B.A., 2014. Shale Gas Potential of the Major Marine Shale Formations in the Upper Yangtze Platform, South China, Part III: Mineralogical, Lithofacial, Petrophysical, and Rock Mechanical Properties. Energy Fuels 28, 2322–2342.

Titiloye, J.O., Skipper, N.T., 2005. Monte Carlo and molecular dynamics simulations of methane in potassium montmorillonite clay hydrates at elevated pressures and temperatures. J. Colloid Int. Sci. 282, 422–427.

Wang, J., Jiang, H., Zhou, Q., Wu, J., Qin, S., 2016. China's natural gas production and consumption analysis based on the multicycle Hubbert model and rolling grey model. Renew. Sustain. Energy Rev. 53, 1149–1167.

Wang, J., Wang, Y., Fan, J., Liu, C., Xue, P., 2015a. Experimental study on coal-bed methane displacement by carbon dioxide injection. Sci. Technol. Rev. 17, 022.

Wang, L., Wang, Z., Li, K., Chen, H., 2015b. Comparison of enhanced coalbed methane recovery by pure N2 and CO_2 injection: Experimental observations and numerical simulation. J. Nat. Gas Sci. Eng. 23, 363–372.

Wu, H., Chen, J., Liu, H., 2015. Molecular Dynamics Simulations about Adsorption and Displacement of Methane in Carbon Nanochannels. J. Phys. Chem. C. 119, 13652–13657.

Youinou, G.J., 2016. Powering sustainable low-carbon economies: Some facts and figures. Renew. Sustain. Energy Rev. 53, 1626–1633.

Yu, H., Yuan, J., Guo, W., Cheng, J., Hu, Q., 2008. A preliminary laboratory experiment on coalbed methane displacement with carbon dioxide injection. Int. J. Coal Geol. 73, 156–166.

Yuan, Q., Zhu, X., Lin, K., Zhao, Y.-P., 2015. Molecular dynamics simulations of the enhanced recovery of confined methane with carbon dioxide. Phys. Chem. Chem. Phys. 17, 31887–31893.

Zeng, F., Huang, W.B., Liu, M., Lu, S.F., Yu, L., 2014. A Study on Quantitative Characterization of Adsorption Capacity of Shale. Adv. Mater. Res., 20–25.

Zhai, Z., Wang, X., Jin, X., Sun, L., Li, J., Cao, D., 2014. Adsorption and Diffusion of Shale Gas Reservoirs in Modeled Clay Minerals at Different Geological Depths. Energy Fuels 28, 7467–7473.

Zhang, T., Ellis, G.S., Ruppel, S.C., Milliken, K., Yang, R., 2012. Effect of organic-matter type and thermal maturity on methane adsorption in shale-gas systems. Org. Geochem. 47, 120–131.